Articles

Ring Slippage vs Charge Transfer in the Reductive Chemistry of [IndMo(CO)$_2$(α-diimine)]$^+$ Cations

Cláudia C. L. Pereira,[†] Paulo J. Costa,[†,‡] Maria José Calhorda,[†,‡] Cristina Freire,[§] Sandra S. Rodrigues,[†,||] Eberhardt Herdtweck,[⊥] and Carlos C. Romão*[,†]

Instituto de Tecnologia Química e Biológica, da Universidade Nova de Lisboa, Av. da República, Estação Agronómica Nacional, 2780-157 Oeiras, Portugal, Departamento de Química e Bioquímica, Faculdade de Ciências, Universidade de Lisboa, Campo Grande, 1749-016 Lisboa, Portugal, REQUIMTE, Departamento de Química, Faculdade de Ciências, Universidade do Porto, R. do Campo Alegre, 4169−007 Porto, Portugal, Alfama, Investigação e Desenvolvimento de Produtos Farmacêuticos Lda., Taguspark, Núcleo central, 267, 2740-122 Porto Salvo, Portugal, and Anorganisch-chemisches Institut der Technische Universität München, Lichtenbergstrasse 4, D-85747 Garching b. München, Germany

Received November 16, 2005

Thirteen complexes of the type [IndMo(CO)$_2$L$_2$]$^+$ were prepared from IndMo(η^3-C$_3$H$_5$)(CO)$_2$ by protonation with HBF$_4$·Et$_2$O followed by addition of α-diimine ligands L, in the presence of 1,2-dimethoxyethane. The complexes are numbered as follows: L = 1,4-bis(*p*-tolyl)diazabutadiene (*p*-tolDAB, **1**), 1,4-bis(cyclohexyl)diazabutadiene (cyDAB, **2**), biquinoline (biq, **3**), 5,6-Ph$_2$-3-(2-py)-1,2,4-Tz (tz, **4**), dipyrido[3,2-*a*:2′,3′-*c*]phenazine (dppz, **5**), 2,2'-bipyridine (bipy, **6**), 4,4′-diphenyl-2,2′-bipyridine (4,4′-Ph$_2$-bpy, **7**), 1,10-phenanthroline (1,10-phen, **8**), 4,7-diphenyl-1,10-phenanthroline (4,7-Ph$_2$-1,10-phen, **9**), 4,7-dimethyl-1,10-phenanthroline (4,7-Me$_2$-1,10-phen, **10**), 2-(2-pyridyl)benzimidazole (2-(2-py)-benz, **11**), 2,2′-biimidazole (2,2′-Biim, **12**), 1,2-phenylenediamine (phendiam, **13**). The bonding mode of the ligand in **4** was ascertained by single-crystal X-ray diffraction. None of the complexes undergo NCMe addition to form ring-slipped [(η^3-Ind)Mo(CO)$_2$L$_2$(NCMe)]$^+$ species. The reductive electrochemistry was studied in order to search for possible reductively induced ring-slippage rearrangements. In the cases of **1**−**5** reversible reduction processes were observed. UV−vis spectroscopy combined with DFT calculations provided an interpretation for the structures of the reduced species. The data suggest that the unpaired electron in the formally 19e reduced products [IndMo(CO)$_2$L$_2$]$^\bullet$ is localized on the α-diimine ligand with minimal structural changes and no indenyl slippage taking place. However, such slippage is predicted to take place with the second reduction step, but in most cases MoL$_2$ bond breaking leads to irreversible electrochemistry.

Introduction

Indenyl slippage can be promoted by two types of processes that vary the electron count at the metal: ligand addition/elimination or redox processes (oxidation/reduction). In the case of the complexes [IndMo(CO)$_2$L$_2$]$^+$ such events are depicted in Scheme 1. Previous studies have shown that NCMe addition is dependent on the nature of the L ligands being favored for π donors: namely, O donors and even NCMe. Computational studies shed some light on the reasons for this behavior and were quantified for the particular case of L = NCMe, CNMe.[1]

Reductively induced ring-slippage events are also expected to be dependent on L, but the final outcome is less predictable. In fact, the radical species formed after addition of the first electron may lead to a 19e complex (**A**), a ring-slipped species (**B**) essentially close to an 18e configuration, or a ligand-centered 18e radical complex (**C**) where the unpaired electron resides on ligand orbitals. In the last case the L ligands act as electron sinks.

In a recent report, Sweigart and co-workers summarize the evidence regarding these cases for Cp/indenyl and arene/polyarene slippage.[2] The 19e radical [η^5-IndFe(CO)$_3$] exemplifies case **A**.[3] The situation described in **B** results from an incomplete slippage toward a $\eta^3 + \eta^2$ bonding mode where the η^2 component lies on the outer bonding distance range (ca. 2.8 Å), as seen along the series Ind$_2$M for M = Fe, Co, Ni. The increasing formal electron count in the order Fe (18e) < Co (19e) < Ni (20e) leads to an increased distortion of the indenyl in the Co and Ni complexes in terms of slippage and bending.[4] A similar situation is observed in the complex [IndCpMo(P{OMe}$_3$)$_2$]$^+$, a formally 19e intermediate in the reversible

[†] Universidade Nova de Lisboa.
[‡] Universidade de Lisboa.
[§] Universidade do Porto.
[||] Alfama, Investigação e Desenvolvimento de Produtos Farmacêuticos Lda.
[⊥] Technische Universität München.

(1) Calhorda, M. J.; Gamelas, C. A.; Gonçalves, I. S.; Herdtweck, E.; Romão, C. C.; Veiros, L. F. *Organometallics* **1998**, *17*, 2597.

(2) Reingold, J. A.; Virkaitis, K. L.; Carpenter, G. B.; Sun, S.; Sweigart, D. A.; Czech, P. T.; Overly, K. R. *J. Am. Chem. Soc.* **2005**, *127*, 11146 and references therein.

(3) Pevear, K. A.; Banaszak Hall, M. M.; Carpenter, G. B.; Rieger, A. L.; Rieger, P. H.; Sweigart, D. A. *Organometallics* **1995**, *14*, 512.

10.1021/om050986r CCC: $33.50
Publication on Web 09/26/2006

Scheme 1

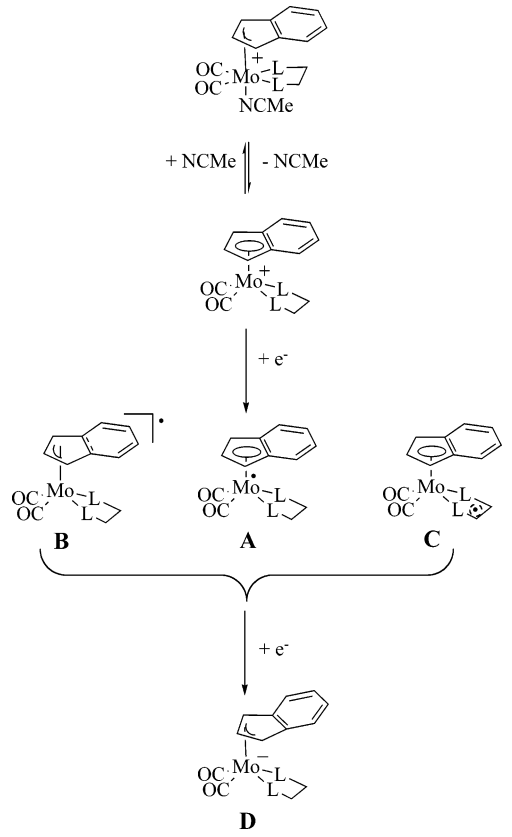

redox pathway between $[IndCpMo(PR_3)_2]^{2+}$ and $[(\eta^3\text{-Ind})CpMo(PR_3)_2]$ ($PR_3 = {}^1/_2$ dppe, $P(OMe)_3$).[5] The reactivity of such radicals may be very high, leading to ligand substitution and/or products derived from ligand-based radicals.[6]

Further reduction by a second electron is not always feasible but in many instances has been achieved, resulting in more clear-cut slippage, namely to η^3-Ind (Scheme 1) and η^4-arene complexes.

Most of these studies have been conducted with hydrocarbon complexes or binary hydrocarbon/CO (PR_3) complexes. The simultaneous introduction of other ligands that might compete with these as electron sinks is less studied.

According to the evidence mentioned above, the radical complexes $[IndMo(CO)_2L_2]$ (L_2 = α-diimine) presented in this work are candidates for undergoing a partial indenyl slippage. However, α-diimine ligands are π-acceptors that may accommodate the "19th electron" gained by the complex upon reduction, as extensively documented in the reductive chemistry of $[Re(CO)_3L(\alpha\text{-diimine})]^+$ complexes.[7] However, the latter lack other competing delocalized π-hydrocarbon ligands. Depending on which electron sink is more effective, the formation of species of type **C** may prevail over type **B** indenyl-slipped species as the means to avoid effective breaking the 18e rule in formally 19e species. Regardless of its structural features, further reduction is most likely to produce a fully η^3-indenyl complex of type **D**. These studies and the results obtained are presented and discussed in this article. A further note that prompted our interest in these studies is the fact that many of the complexes presented here are the first cytotoxic molybdenum carbonyls described and are undergoing development as antitumor agents.[8]

Scheme 2

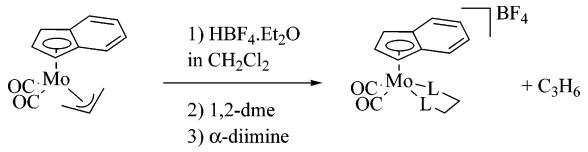

Results

Synthesis. The preparation of the complexes $[(\eta^5\text{-Ind})Mo(CO)_2L_2]BF_4$ (**1**−**13**) is based upon previous methods developed in this group and summarized in Scheme 2. The intermediate use of the 1,2-dme complex (produced in situ and never isolated) allows a cleaner separation of the final products before recrystallization.

Of the 13 compounds prepared by this route (Chart 1) only one (**6**) had been previously reported.[9]

The compounds have a common piano-stool structure with two cis CO ligands and one η^5-ind ring. The cis configuration of the CO ligands produces the two IR stretching vibrations, except for **3**, where the four vibrations are assigned to the two isomers **3a**,**b** as already reported for $[IndMo(CO)_2(CNMe)_2]^+$.[1]

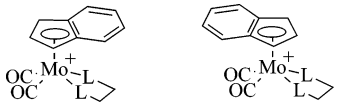

(**3a**) (**3b**)

The IR data show that the DAB ligands are the strongest π-acceptors, since they present the highest ν(CO) values. Remarkably, the *p*-tolDAB ligand (**1**; ν(CO) 2019, 1976 cm^{-1}) exerts a π-accepting effect far stronger than that measured for the isonitrile ligand CNMe, which shows ν(CO) values at 1995 and 1927 cm^{-1}. The latter values are essentially the same present in the cyDAB complex **2** (ν(CO) 1994, 1928 cm^{-1}) and are between 12 and 61 cm^{-1} higher than those of all other complexes **3**−**13**.

The typical resonance patterns for the η^5-indenyl protons in $[(\eta^5\text{-Ind})Mo(CO)_2L_2]^+$ complexes have been previously identified and reported.[1] In those complexes with symmetric nitrogen ligands such as **1**, **2**, **7**, **12**, and **13**, the resonance pattern for the indenyl ring protons in ^1H NMR includes two sets of signals (7.59−6.28 ppm) attributed to H^{5-8} (C6 ring protons), a doublet (6.63−6.06 ppm) for $H^{1/3}$, and a triplet (5.52−5.19 ppm) for H^2 (see Figure 1 for indenyl atom numbering). The ^1H NMR spectrum of **3** (two isomers by IR in KBr) only shows one set of resonances, suggesting that the indenyl rotation becomes fast on the NMR time scale at room temperature.

A different pattern of resonances was observed for the dppz- and phenanthroline-derived complexes **5** and **8**−**10**. In all of these complexes, the signal for $H^{1/3}$ is clearly shifted

(4) (a) Westcott, S. A.; Kakkar, A. K.; Stringer, G.; Taylor, N. J.; Marder, T. B. *J. Organomet. Chem.* **1990**, *394*, 777. (b) Calhorda, M. J.; Veiros, L. F. *J. Organomet. Chem.* **2001**, 635, 197−203.

(5) Stoll, M.; Belanzoni, P.; Calhorda, M. J.; Drew, M.; Félix, V.; Geiger, W. E.; Gamelas, C. G.; Gonçalves, I. S.; Romão, C. C.; Veiros, L. F. *J. Am. Chem. Soc.* **2001**, *123*, 10595.

(6) Amatore, C.; Ceccon, A.; Santi, S.; Verpeaux, J. N. *Chem. Eur. J.* **1997**, *3*, 279.

(7) (a) Sun, S. S.; Lees, A. J. *Coord. Chem. Rev.* **2002**, *230*, 171. (b) Schoonover, J. R.; Strouse, G. F. *Chem. Rev.* **1998**, *198*, 1335. (c) Stufkens, D. J.; Vlček, A. *Coord. Chem. Rev.* **1998**, *177*, 127.

(8) Matos, M. R. P. N.; Romão, C. C.; Pereira, C. C. L.; Rodrigues, S. S.; Mora, M.; Silva, M. J. P.; Alves, P. M.; Reis, C. A. Compositions Comprising Organometallic Molybdenum Compounds for Treating Cancer. WO 2005/087783 A1, 2005.

(9) Gamelas, C. G. Ph.D. Dissertation, Instituto de Tecnologia Química e Biológica, Oeiras, Portugal, 2000.

Chart 1. Structures of the Ligands in Complexes 1−13 with Atom Numbering

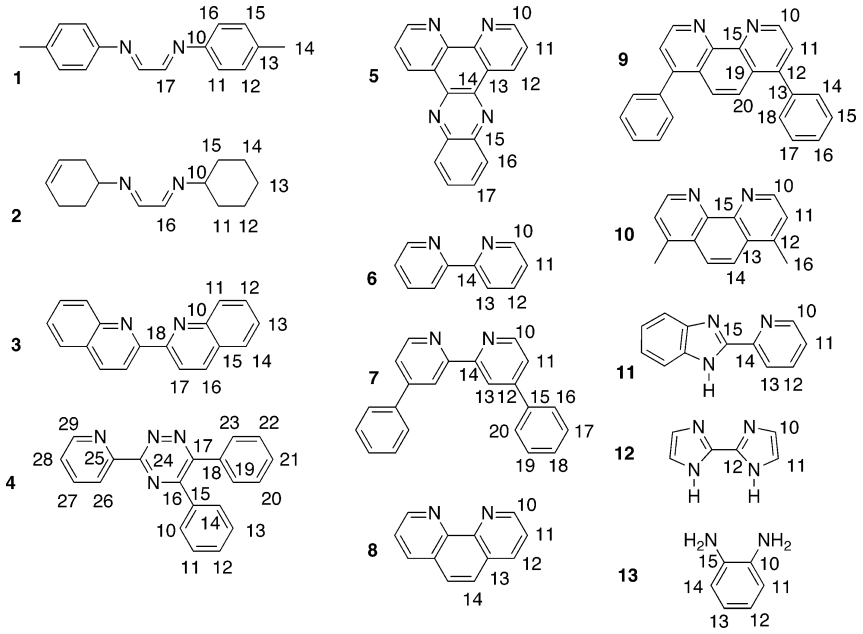

Table 1. Selected Interatomic Distances (Å) and Angles (deg) of Complex 4

Mo−C1	2.286(3)	Mo−N11	2.215(2)
Mo−C2	2.269(3)	Mo−N21	2.168(2)
Mo−C3	2.291(3)	Mo−C8	1.967(2)
Mo−C3A	2.408(2)	Mo−C9	1.985(3)
Mo−C7A	2.409(3)		
N11−Mo−N21	72.73(7)	N21−Mo−C8	127.0(1)
N11−Mo−C8	83.37(9)	N21−Mo−C9	81.4(1)

downfield and appears somewhere between the two multiplets of H$^{5-8}$, which are themselves also rather deshielded. This shift certainly originates in the aromatic ring currents of the phenanthroline ligands that lie face-to-face with the C6 ring of the indenyl ligand.

Asymmetric ligands such as those in **4** and **11** induce metal-centered chirality with diastereotopic resonances for indenyl rings much more complicated than those presented before. This is particularly complex for the triazine complex **4** (not shown). Despite extensive NMR characterization, we were unable to assign the coordination mode of this multidentate ligand from the two existing possibilities. This structural assignment was only unequivocally accomplished using single-crystal X-ray diffraction, as depicted in Figure 1 and Table 1.

The structure evidences the four-legged piano-stool structure typical of this family of complexes, with the η^5 coordination mode of the C5 ring of the indenyl ligand. As expected from Faller's rule of thumb, the C6 moiety of the indenyl ring occupies the position trans to the two CO ligands.[10] As has been calculated, this is the thermodynamically favored orientation, but the energetic barrier for rotation is not very high.[5]

This structure corresponds to the most favorable steric interaction between the triazine ligand and the IndMo(CO)$_2$ fragment. The other alternative would place a phenyl substituent too close to the other ligands in the coordination sphere.

NCMe Addition to Complexes 1−13. In contrast to the [IndMo(CO)$_2$L$_2$]$^+$ complexes with π-donor ligands such as L = NCMe, OPPh$_3$, OP(OMe)$_3$, acac, where the addition of acetonitrile induces ring slippage,[1] in all of the new compounds **1−13** no such slippage was detected by ^{1}H NMR analysis performed in NCCD$_3$.

Electrochemical Studies. The oxidative and reductive electrochemical properties of all monocations **1−13** were studied in CH$_2$Cl$_2$ by cyclic voltammetry; the corresponding data are summarized in Table 2. All of the compounds display irreversible oxidation processes at high positive potential values (E_a > 0.8 V).

In the series of homologous neutral complexes IndMo(CO)$_2$(LX) (LX = carboxylate, amidinate, acac, S$_2$P(OEt)$_2$), the compound IndMo(CO)$_2$(S$_2$P(OEt)$_2$) showed a reversible Mo(II) → Mo(III) oxidation process at $E_{p,1/2}$ = +0.44 V.[9] Although the irreversible nature of the oxidation process in the compounds prepared within this work prevents a straightforward comparison with data for IndMo(CO)$_2$(LX) complexes, their irreversible oxidation processes can be tentatively assigned to an oxidation reaction involving ultimately the Mo center, in agreement with the Mo−CO bonding nature of the HOMO (see below).

The reductive electrochemical properties of the complexes are quite disparate. Among all the complexes **1−13,** five of them (**1−5**) showed reversible reduction processes in the region −0.39 to −0.97 V. Complex **1** is the only one that shows two reversible reduction processes separated by 0.58 V (Figure 2), and compounds **2−5** present one reversible process with $E_{1/2}$ values in the range −0.69 to −0.87 V, somewhere between the two redox processes observed for compound **1**; furthermore, complexes **3** and **5** have a second irreversible reduction at more negative potentials, E_p < −1.1 V. All of the other complexes show irreversible processes in the range −0.93 to −1.40 V, with the exception of complex **12**, which has irreversible reduction processes at less negative potentials: ca. −0.29 and −0.18 V. No further characterization was pursued for complexes **6−13**, as all of their reduction processes are irreversible.

UV−Vis Electronic Spectra. To get information on the electronic and structural changes undergone by the complexes upon reduction, UV−vis spectra were obtained for the complexes that showed at least one reversible reduction process (**1−4**). The electronic spectra of the reduced species were obtained in NCMe after the electrolysis of the complexes at fixed potentials, as described in the Experimental Section; given the difference in coordinating power between this solvent and CH$_2$Cl$_2$, some of the conclusions must, therefore, be regarded with

(10) Faller, J. W.; Crabtree, R. H.; Habib, A. *Organometallics* **1985**, *4*, 929.

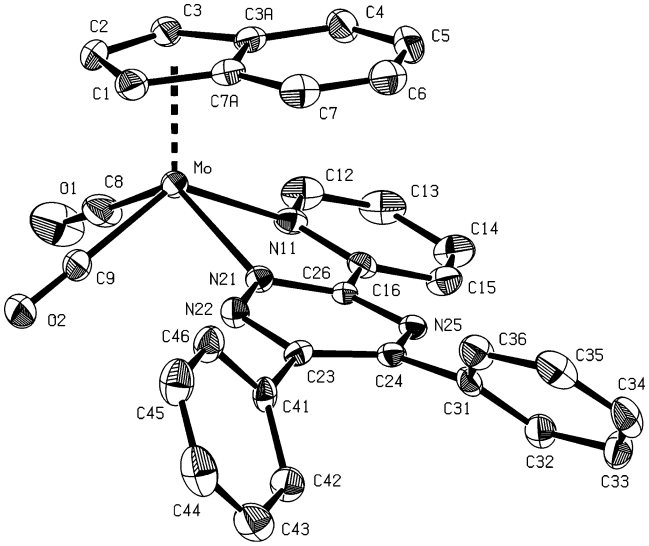

Figure 1. Ortep style plot of the solid-state structure of compound **4**. Thermal ellipsoids are drawn at the 50% probability level. The hydrogen atoms are omitted for clarity.

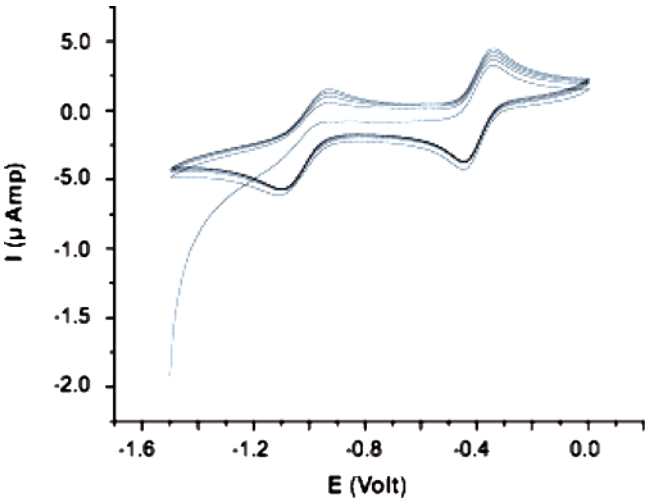

Figure 2. Cyclic voltammogram of [IndMo(CO)$_2$(*p*-tolDAB)]BF$_4$ (**1**) in CH_2Cl_2/0.1 M $TBABF_4$ at 0.25 V/s, in the region +0.20 to −1.5 V.

caution. In this context, the UV−vis spectra of the complexes **1**−**4** were recorded in NCMe and compared with those of the reduced species generated electrolytically at −1.25 V; for complex **1**, the electronic spectrum of the reduced species at −0.75 V was also recorded, as this complex has a second reduction process at a less negative potential. The spectra of the free ligands were also measured in NCMe for comparison; data on the spectrum of the reduced *p*-tolDAB ligand in NCPr were taken from ref 11.

The complexes **1**−**4** (before the electrolysis) show, in the region λ 500−600 nm, electronic bands that are assigned to metal-to-ligand charge transfer (MLCT) transitions, which determine their colors, confirmed by the values of the extinction coefficients determined for complex **1**: for λ_{max} 585 nm ϵ = 1900 mol^{-1} dm^3 cm^{-1}. They also show at λ < 350 nm very intense bands (3000 < ϵ < 3800 mol^{-1} dm^3 cm^{-1}) which can be assigned to ligand-centered (LC) transitions,[12,13] as they appear at almost the same wavelengths as those of the free ligands.

Table 2. Cyclic Voltammetric Data for the Complexes [IndMo(CO)$_2$L$_2$]$^+$ [a]

	redn process					oxidn process
complex, ligand	$E_{p,c}$	$E_{p,a}$	ΔE	$E_{p,1/2}$	i_a/i_c	$E_{p,a}$
1, *p*-tol-DAB	−0.44	−0.34	0.10	−0.39	1.0	1.31
	−1.04	−0.94	0.10	−0.97	1.0	
2, CyDAB	−0.79	−0.69	0.10	−074	0.92	1.22
3, Biq	−0.74	−0.64	0.10	−0.69	1.0	1.17
	−1.12	irr				
4, Tz	−0.82	−0.65	0.17	−0.73	1.0	1.04
						1.27
5, Dppz	−0.91	−0.83	0.08	−0.87	1.1	1.34
	−1.32	irr				
6, Bipy	−0.93	irr				0.20
	−1.32	irr				1.04
7, Ph_2bpy	−1.07	irr				1.12
8, Phen	−1.15	irr				1.10
9, Ph_2phen	−1.10	irr				1.06
10, Me_2phen	−1.04	irr				0.90
11, pybenz	−1.05	irr				1.03
	−1.37	irr				
12, H_2biim	−0.29	−0.183			irr	0.88
						1.26
13, Phendiam[b]	−1.23	irr				0.83
	−1.49	irr				1.38

[a] Conditions: measurements in CH_2Cl_2/0.1 M $TBABF_4$, unless otherwise specified; scan rate 0.250 V/s; glassy-carbon electrode; Fc^+/Fc redox potential (+0.444 V). $E_{p,a}$, $E_{p,c}$, and $E_{p,1/2}$ are referenced to SCE. All *E* values are given in V. [b] Measurements in 1,2-dme.

Table 3. Electronic Band Maxima (λ_{max}, nm (ϵ, mol^{-1} dm^3 cm^{-1})) for Complex 1: before (1$^+$) and after Electrolysis at −0.75 V (1), after Electrolysis at −1.5 V (1$^-$), and Free Ligand (*p*-Tolyl-1,4-diazabutadiene)

before electrolysis	after electrolysis at −0.75 V	after electrolysis at −1.5 V	free ligand
287 (3500)	238 (4000)	238 (4000)	242
313 (3600)	294 (3700)	294 (3500)	290
415 (3100)	393 (2700)	394 (2000)	348
585 (1900)	548 (1200)		

Complex **1** is probably the most interesting case in this series, because it shows two reversible reduction processes in CH_2Cl_2. In NCMe the UV−vis spectrum of the complex shows very intense bands in the visible region at λ 585 nm (ϵ = 1900 mol^{-1} dm^3 cm^{-1}) and 415 nm (ϵ = 3100 mol^{-1} dm^3 cm^{-1}) and in the UV region at λ 313 nm (ϵ = 3600 mol^{-1} dm^3 cm^{-1}) and 287 nm (ϵ = 3500 mol^{-1} dm^3 cm^{-1}). After electrolysis at −0.75 V the solution shows only small changes in the λ_{max} and ϵ values of these bands, as summarized in Table 3: the solution color changes from deep purple to green and the visible electronic bands shift to higher energies of λ 393 and 548 nm, respectively. These small changes suggest that the reduced species [IndMo(CO)$_2$(*p*-tolDAB)]$^\bullet$ (**1**$^\bullet$) retains all ligands present in the cationic species **1**$^+$. However, this species is not very stable and decomposes at room temperature, as registered by the changes observed in electronic spectra measured within 5 min intervals (Figure 3). Subsequent electrolysis at −1.5 V results in an almost colorless solution, with the same absorption band profile as that of the free ligand, suggesting that the reduced species decomposes into unknown species and free ligand *p*-tolDAB. The spectral data are summarized in Table 4.

The electronic band maxima for compounds **2**−**4** in the UV−vis region, before electrolysis and after electrolysis, are summarized in Table 4; the spectra of the free ligands have been also included.

(11) Rossenaar, B. D.; Hartl, F.; Stufkens, D. J. *Inorg. Chem.* **1996**, *35*, 6194.

(12) Rein, F. N.; Rocha, R. C.; Toma, H. E. *J. Electroanal. Chem.* **2003**, *541*, 103.

(13) Scott, S. M.; Gordon, K, C. *Inorg. Chem.* **1996**, *35*, 2462.

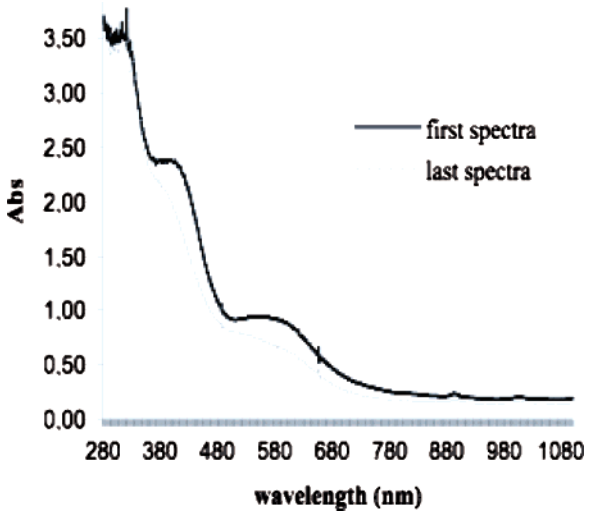

Figure 3. Electronic spectra of reduced [IndMo(CO)$_2$(*p*-tolDAB)]$^+$ at −0.75 V, taken within 5 min intervals.

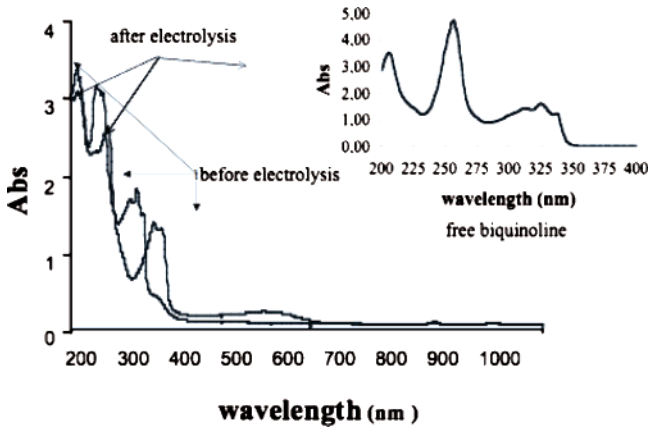

Figure 4. Electronic spectra in the region λ 1000−200 nm for [IndMo(CO)$_2$(Biq)]BF$_4$ (**3**) in NCMe, before and after electrolysis, and for the free ligand (insert).

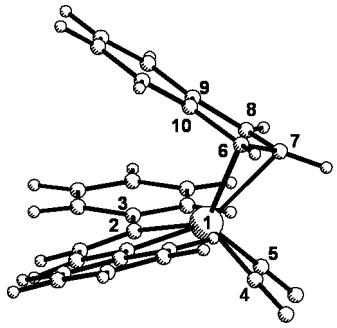

Figure 5. Calculated (ADF) structure of the model direduced complex [IndMo(CO)$_2$(*p*-phDAB)]$^-$ (**1m**$^-$).

As an example, the spectra of complex **3** are depicted in Figure 4: for this particular case the lower energy band at λ 578 nm is assigned to MLCT, involving dπ (Mo) → π* (Biq), and the bands at λ 270 and 216 nm, as they appear at almost the same wavelength of those of the free ligand, are assigned to ligand-centered (LC) transitions.[12,13]

After the electrochemical reduction at −1.25 V the UV−vis spectrum of the reduced complex has the same absorption band profile as that of the free biquinoline ligand (Figure 4), suggesting that the reduced species **3**$^\bullet$ decomposes into unknown species and free biquinoline, as is the case for complex **1** when the electrolysis is carried out at the more positive potential.

Table 4. Electronic Band Maxima (λ_{max}, nm) for Compounds 2−4 in the UV−Vis Region: (A) before Electrolysis; (B) after Electrolysis; (C) Free Ligand

[IndMo(CO)$_2$-(cyDAB)]$^+$ (**2**)			[IndMo(CO)$_2$-(2,2′-Biq)]$^+$ (**3**)			[IndMo(CO)$_2$-(Tz)]$^+$ (**4**)		
A	B	C	A	B	C	A	B	C
214	216	213	216	210	205	208	238	232
239	248	278	270	257	255	292	272	279
272	366		358	313	311	568		
379			373	325	323			
474			578	338	335			
561								

Table 5. Relevant Distances (Å) and Angles (deg) of [IndMo(CO)$_2$(*p*-phDAB)]$^+$ (1m$^+$, 1m$^\bullet$, and 1m$^-$)

distance/angle	**1m**$^+$	**1m**$^\bullet$	**1m**$^-$
Mo−N2	2.232	2.244	2.205
Mo−N3	2.227	2.236	2.197
Mo−C4	1.993	1.968	1.968
Mo−C5	1.990	1.964	1.964
Mo−C6	2.324	2.339	2.381
Mo−C7	2.292	2.291	2.276
Mo−C8	2.327	2.337	2.373
Mo−C9	2.487	2.570	2.800
Mo−C10	2.482	2.566	2.795
folding[a]	5.4	7.7	12.9

[a] Angle between C7, the middle of the C6−C8 bond, and the middle of the C9−C10 bond (Figure 5).

Complex **4** behaves similarly after electrolysis: the ligand triazine is liberated after reduction, as the electronic bands of the electrolyzed solution coincide with those of its free ligand. It should also be pointed out that at −1.25 V there is no reduction of these free diimine ligands in NCMe, since they occur at clearly more negative potentials to form radical anions.[11] The electronic spectrum of the electrolyzed complex **2**, with the cyDAB ligand, is less clear cut; nevertheless, it is obvious that the low-energy bands in the visible region also disappear after electrolysis, suggesting that the Mo−cyDAB bond is also cleaved, but there is still an unassigned electronic band at λ 366 nm.

DFT Calculations. DFT calculations (ADF and Gaussian98; see the Experimental Section for details) were performed in order to understand the UV−vis spectra and the redox behavior of the complexes. The complex [IndMo(CO)$_2$(*p*-tol-DAB)]$^+$ (**1**)- is the most interesting for a deeper study, since it exhibits two separated reduction processes and there are spectral data (UV−vis spectrum) characterizing the reduced species, allowing a comparison between theory and experiment. Therefore, calculations were performed on [IndMo(CO)$_2$(*p*-phDAB)]$^+$ (**1m**$^+$), a model compound for [IndMo(CO)$_2$(*p*-tol-DAB)]$^+$, where the tolyl groups were replaced by phenyl groups. The geometries of the parent cation **1m**$^+$, the neutral monoreduction product **1m**$^\bullet$, and the direduced monoanion **1m**$^-$ were fully optimized (ADF), without symmetry constraints. The most relevant distances and angles are collected in Table 5, and the geometry of the anion is shown in Figure 5, with the numbering scheme.

In the parent complex **1m**$^+$, the Mo−C distances are typical of the $\pi\ \eta^3 + \eta^2$ coordination mode of an indenyl. After the addition of one electron, they remain almost unchanged, with a very small lengthening (**1m**$^\bullet$). The same thing happens with the Mo−N distance, but there is a tendency to shorter Mo−C(O) bonds.

The cation **1m**$^+$ has a relatively low energy LUMO, only 1.374 eV higher than the HOMO, the LUMO+1 being higher by a similar amount (1.413 eV), followed by closely spaced levels. The monoreduced complex is paramagnetic, while the

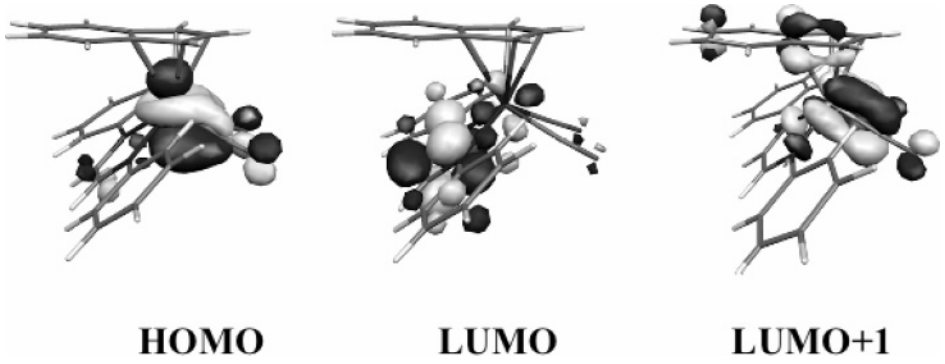

Figure 6. Frontier orbitals (Gaussian) of the cation $[IndMo(CO)_2(p\text{-phDAB})]^+$ (**1m**$^+$) in a MOLEKEL representation.

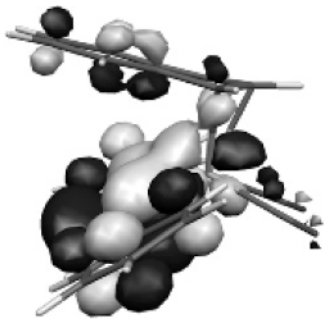

Figure 7. HOMO (Gaussian) of the anion **1m**$^-$.

second electron, in the direduced species **1m**$^\bullet$, can occupy the same level or the next one, giving rise to a singlet or a triplet species. It was found (ADF) that the singlet was more stable than the triplet by 18 kcal mol^{-1}. Therefore, the monoanion **1m**$^-$ was considered to be diamagnetic, with two electrons in the LUMO, rather than paramagnetic with two unpaired electrons: one in LUMO and one in LUMO+1. The frontier orbitals of the cation **1m**$^+$ are depicted in Figure 6, in a MOLEKEL representation.

There are two interesting features of the anion **1m**$^-$: the persistent orientation of the indenyl group and its small slippage. The benzene ring of the indenyl group stays over the DAB ligand after mono- and direduction, in opposition to what has been found in most systems (see below).[10] Among the Mo−C distances to the indenyl carbons (Table 5), two are significantly longer (2.800, 2.795 Å) than in the cation (2.487, 2.482 Å) and the radical (2.570, 2.566 Å). These distances to the junction carbons are typical of what we called coordination between η^3 and η^5. This amount of slippage is not expected from full occupation of the LUMO, as shown in Figure 6, and, as a matter of fact, the degree of slippage is also small. Note the folding angle of 12.9°, compared with 5.4° (**1m**$^+$) and 7.7° (**1m**$^\bullet$). Interestingly, this bending and the Mo−C(indenyl) distances are very similar to those calculated for the radical cation $[IndCpMo\{(POMe_3)_2]^+$ with only one unpaired electron.[5] The LUMO of **1m**$^+$ is very similar to both the SOMO of **1m**$^\bullet$ and the HOMO of **1m**$^-$, shown in Figure 7, with a smaller wave function contour. The participation of the indenyl ring becomes visible. Indeed, although this is mostly a π^* orbital of the DAB, the Mo−C(O) bonding character is visible and is enhanced by slippage, as described in other examples.[14] It would be Mo−C(indenyl) antibonding in **1m**$^+$, but ring slippage makes it Mo−C(indenyl) bonding in **1m**$^-$ and, therefore more stable. The small slippage and bending reflect the fact that this orbital is mainly DAB π^*, rather than Mo−indenyl. Indeed, DAB π^* contributes 74.5% to this HOMO, Mo contributes 12.4%, the indenyl ring contributes 11.4%, and the carbonyls contribute 1.7%.

Table 6. Calculated Low-Energy Singlet Excitation Energies, Wavelengths, and Oscillator Strengths (OS) of $[IndMo(CO)_2(phDAB)]^+$ (1m$^+$), $[IndMo(CO)_2(phDAB)]^\bullet$ (1m$^\bullet$), and $[IndMo(CO)_2(phDAB)]^-$ (1m$^-$)

composition	energy (eV)	wavelength (nm)	λ_{max} (nm)	OS
	1m$^+$			
32% (H-3 → L), 8% (H → L)	2.402	516	585	0.055
36% (H-1→L)	2.675	464	415	0.478
	1m$^\bullet$			
92% (H-1$_\beta$ → L$_\beta$)	2.200	563	548	0.128
36% (H$_\alpha$ → L+3$_\alpha$), 29% (H-2$_\beta$ → L+2$_\beta$)	3.047	407	393	0.097
41% (H$_\alpha$ → L+3$_\alpha$), 18% (H-2$_\beta$ → L+2$_\beta$)	3.095	401		0.098
	1m$^-$			
38% (H → L)	1.748	709		0.059
32% (H → L+2), 10% (H → L+4)	2.974	417		0.097

TD-DFT[15] calculations were performed for the three species with Gaussian98, and ADF was used for the closed-shell systems, the results being similar in these cases. Only the Gaussian data will be given. The contributions, characters, and oscillator strengths of the most intense transitions for the three model complexes **1m**$^+$, **1m**$^\bullet$, and **1m**$^-$ are collected in Table 6.

There are two stronger bands for the cation, at 516 and 464 nm, comparing relatively well with the observed ones at 585 and 415 nm. The main component of the low-energy band (516 nm) can be assigned to a metal to π^* transition in the DAB ligand (MLCT), since both H and H-3 are essentially metal d. Note that the HOMO is not involved in this transition and that the end point is always the LUMO. The orbitals involved in this transition are represented in Figure 8 (left). The transition at 464 nm derives primarily from excitations starting in H-1 (DAB π) and ending in the LUMO (DAB π^*, ligand-centered transition). The low-energy LUMO is strongly populated by the excitations. This ligand has a strong acceptor capability, being competitive even with CO, as noted earlier in the CO stretching frequencies. The orbitals involved in these transitions are represented in Figure 8 (right).

(14) (a) Calhorda, M. J.; Veiros, L. F. *Coord. Chem. Rev.* **1999**, *185*−*186*, 37. (b) Calhorda, M. J.; Veiros, L. F. *Comments Inorg. Chem.* **2001**, *22*, 375.

(15) (a) Stratmann, R. E.; Scuseria, G. E.; Frisch, M. J. *J. Chem. Phys.* **1998**, *109*, 8218−8224. (b) Bauernschmitt, R.; Ahlrichs, R. *Chem. Phys. Lett.* **1996**, *256*, 454−464. (c) Casida, M. E.; Jamorski, C.; Casida, K. C.; Salahub, D. R. *J. Chem. Phys.* **1998**, *108*, 4439−4449. (d) van Gisbergen, S. J. A.; Groeneveld, J. A.; Rosa, A.; Snijders, J. G.; Baerends, E. J. *J. Phys. Chem.* **1999**, *103A*, 6835. (e) Rosa, A.; Baerends, E. J.; van Gisbergen, S. J. A.; van Lenthe, E.; Groeneveld, J. A.; Snijders, J. G. *J. Am. Chem. Soc*. **1999**, *121*, 10356. (f) van Gisbergen, S. J. A.; Rosa, A.; Ricciardi, G.; Baerends, E. J. *J. Chem. Phys.* **1999**, *111*, 2499.

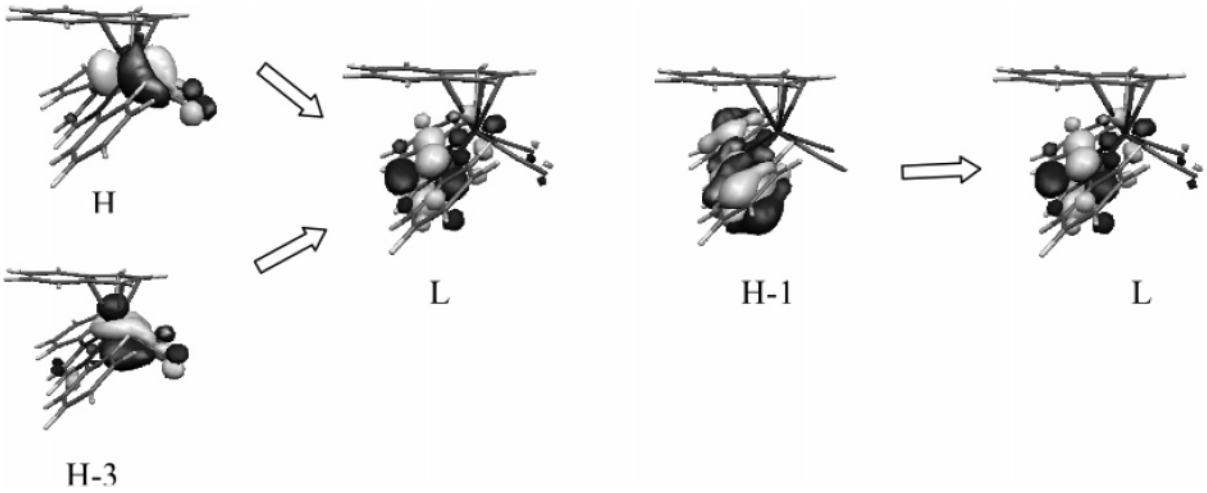

Figure 8. Orbitals involved in the two transitions calculated at 516 nm (left) and 464 nm (right) for the cation **1m**$^+$.

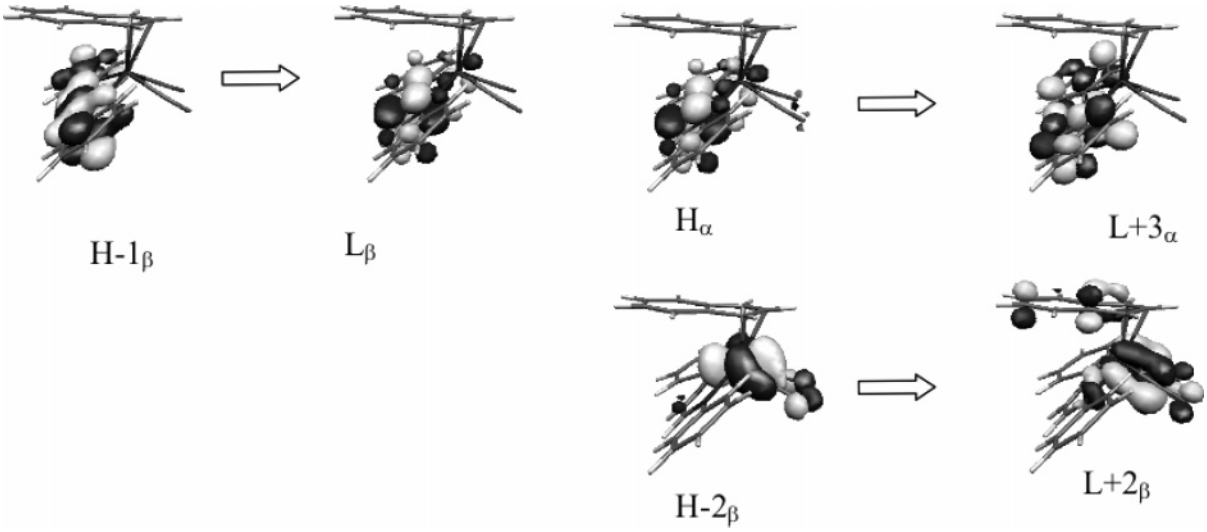

Figure 9. Orbitals involved in the two transitions calculated at 563 nm (left) and 407 and 401 nm (right) for **1m**$^\bullet$.

The results of similar calculations performed for the radical **1m**$^\bullet$ are also presented in Table 6. The lowest energy band is calculated to appear at 563 nm, very close to the experimental value of 548 nm. This transition starts in H-1$_\beta$, essentially DAB π, and ends in the β LUMO (DAB π*). It can be assigned as a ligand-centered transition, and the relevant orbitals involved in the transition are depicted in Figure 9 (left). This radical also has a higher energy band in the visible region at 393 nm, comparing very well with the predicted two excitations at 401 and 407 nm. The α contribution starts in the HOMO (mostly DAB π*) and ends in the LUMO (mostly DAB π*), and the β contribution is mainly metal centered (dd and metal to CO and indenyl). This transition is therefore of the ligand-centered type with some mixture of MLCT (L being CO and indenyl). The relevant orbitals involved in the transition are depicted in Figure 9 (right).

The deviations found between the calculated wavelengths and the experimental ones are within the errors usually accepted for these calculations that, inter alia, do not take solvent effects into account. They support the idea that the monoreduced species is the radical complex **1m**$^\bullet$. Both the calculated and the observed bands are shifted compared to those of the parent **1m**$^+$.

The results of the calculations performed for the anion **1m**$^-$ are also presented in Table 6. The predicted UV−vis bands would be found at 709 and 417 nm. They involve metal d contributions and DAB π* and bear no relation to the experimental UV−vis spectrum obtained after **1m**$^+$ is electrolyzed at −1.50 V, confirming the idea that the complex has decomposed, liberating the anion.

Discussion

The goal of the present work was the study of the indenyl slippage in the complex cations [IndMo(CO)$_2$(α-diimine)]$^+$. The presence of these N-heterocyclic ligands adds uncertainty to any prediction based upon our previous work on [IndMo^{II}(CO)$_2$] derivatives and to those of others on hydrocarbon-only and hydrocarbon/CO complexes.[2,3,6] The fact that none of the complexes **1**−**13** undergo indenyl slippage to octahedral [(η^3-Ind)Mo(CO)$_2$L$_2$(NCMe)]$^+$ upon dissolution in NCMe is now readily explained by the DFT studies. Indeed, ring slippage by ligand addition requires the LUMO to be metal−ring antibonding, so that it can be stabilized upon slippage. Such is not the case (at least to a great extent) in these series of complexes. As seen in Figure 6, the LUMO is essentially located at the DAB ring without contribution from the indenyl ring. Interestingly, the results remain in line with the qualitative interpretation that only weak π-acceptor L ligands favor ligand-induced indenyl slippage in the [IndMo(CO)$_2$L$_2$]$^+$ complexes.

The same molecular orbital picture is now the basis for the interpretation of the experimental results on the attempted reductively induced ring slippage probed by our electrochemical

Scheme 3

IR ν(CO) cm-1: *p*-tolDAB > cyDAB > Tz > Biq > dppz

increasing electron richness

1st reduction V: *p*-tolDAB >> Biq > cyDAB > Tz > dppz

increasing difficulty of reduction

and spectroelectrochemical studies. Although it has no relevance to ring-slippage events, one should note that all of the complexes **1**−**13** are only oxidized at relatively high positive potentials in an irreversible manner. From these, only five complexes showed reversible reduction processes at negative potentials. The ease of reduction correlates fairly well with the order of electron richness, as measured qualitatively from the ν(CO) stretching frequencies and sketched in Scheme 3.

It is known that 1,4-diaza-1,3-butadienes (DAB) are, in general, simultaneously strong σ-electron donors and π-acceptors due to the low-lying π^* orbitals.[16,17] This enhanced π-accepting capability compared to that of the other heterocyclic diimines used here (e.g., Phen, Tz, and Biq) is clearly reflected by the higher CO stretching frequencies of complexes **1** and **2**. The most obvious mismatch between both orders in Scheme 3 concerns the cyDAB ligand. This apparent misplacement, however, finds precedent, for instance, in the pair of complexes [ReBr(CO)$_3$(cyDAB)] and [ReBr(CO)$_3$(*p*-tolDAB)]: the IR vibrations are rather similar in energy, with a slightly higher frequency and force constant for the more electron withdrawing *p*-tolDAB derivative, but the difference in the reduction potentials for both complexes is 0.350 V, the *p*-tolDAB derivative being easier to reduce.[11] This difference equals that reported in this work between $E_{1/2}$ values of **1** and **2,** which also differ by 0.35 V for the first reduction, again easier for the *p*-tolDAB derivative **1**$^\bullet$ (Table 2). Certainly, this mismatch reflects an increased stabilization of the reduced products by the *p*-tolDAB ligand, which facilitates both redox processes exhibited in the cyclic voltamogramms of **1** (Figure 2), probably due to stabilization of the excess charge over the phenyl substituents.[18] We will come to this point later on.

Although complexes **3**−**5** show reversible reduction processes, they decompose during their electrolytic reduction, as deduced by the colorless solutions formed, which coincide with the free ligand spectra. This indicates that the reduced species are unstable on the time scale of the electrolysis, precluding any attempt at characterization. The structures of the reduced species **1** and **2** were studied by means of UV−vis spectroelectrochemistry although limited to the use of NCMe.

In the case of complex **1** the first reduction was observed at $E_{p,1/2} = -0.44$ V in CH_2Cl_2 (Scheme 1). To complement the electronic spectral data, we used DFT calculations to support the assignment of the electronic bands, simultaneously optimizing the structure of the species involved.

In these calculations, the structure of a model of the purple cation **1**$^+$ (**1m**$^+$) was first optimized. This model, **1m**$^+$, uses the phDAB ligand, which only differs from *p*-tolDAB in the absence of the *p*-CH_3 substituent. We reasoned that this small difference would not affect the conclusions of the calculations to a large extent. The calculated (both Gaussian and ADF, not shown) UV−vis spectrum of **1m**$^+$ is indeed in rather good agreement with the experimental data (Table 6), providing safe ground for further studies. The band at 464 nm is essentially ligand-based with contributions from intraligand $\pi \rightarrow \pi^*$ transitions centered on the DAB ligand. MLCT dominates the band at lower energy (516 nm). Upon electrolytic reduction at −0.75 V the new green reduction product, the radical **1**$^\bullet$, also presents two similar absorption bands in the visible region. The incoming electron should enter the LUMO of the initial cation **1m**$^+$, which has no contribution from the indenyl ligand (Figure 6) and is mainly localized on the DAB ligand. Therefore, the very strongly π-accepting *p*-tolDAB ligand takes up the extra 19th electron with very little disturbance of the structure of the fragment [IndMo(CO)$_2$]$^+$, as can be seen on comparing the structures and bond distances (Table 5) calculated for the model phDAB complex. In agreement with this observation, both visible bands of **1**$^\bullet$ are largely dominated by transitions ending in the DAB π^* LUMO (Table 6 and Figure 9). In terms of formal oxidation states we can then consider **1**$^\bullet$ as an [IndMo^{II}(CO)$_2$]$^+$ derivative of the radical anion ligand [*p*-tolDAB]$^{\bullet-}$. The related radical anion [ReBr(CO)$_3$(*p*-tolDAB)]$^{\bullet-}$ has been described in a similar fashion.[11] This kind of electronic arrangement classifies the radical intermediate **1**$^\bullet$ as a ligand-delocalized (18 + δ)-electron complex.[19] In many cases such electronic situations entail distortion of the ligands such as bending (CO, NO) or slippage (Cp).[20] Despite the presence of the structurally flexible indenyl ligand, no significant structural changes are observed or computed.

At more negative potentials, **1**$^\bullet$ undergoes further reduction to **1**$^-$, a process that is reversible on the CV time scale but leads to decomposition under electrolytic conditions. This decomposition liberates the DAB ligand. However, on consideration of the second reduction there are two possibilities to accommodate the incoming electron: as a second electron in the SOMO orbital of **1**$^\bullet$ (the LUMO of **1**$^+$) or as a second unpaired electron in the LUMO of **1**$^\bullet$ (the LUMO+1 of **1**$^+$). According to the calculations on **1m**$^-$ the first hypothesis is energetically preferred, predicting the diamagnetic anion **1**$^-$. According to Figure 6 (center), the LUMO of **1m**$^+$ has no indenyl participation and, therefore, one might expect the formally 20e complex anion **1m**$^-$ as a derivative of [IndMo^{II}(CO)$_2$]$^\bullet$ and the monoanion [phDAB]$^{\bullet-}$. However, the HOMO of **1m**$^-$ is different from the LUMO of **1m**$^+$, owing to electron repulsion, and has a small participation from the indenyl ring, allowing indenyl slippage away from the η^5 coordination mode toward an intermediate coordination between η^5 and η^3. In **1m**$^-$ the Mo−C distances to the junction C atoms between the C5 and C6 rings of the indenyl are rather elongated (ca. 2.8 Å) and there is a clear bending of the ring along the hinge C atoms at the end of the pseudo-allylic moiety more closely bonded to the Mo atom (12.9°). These distances are close to those reported for other 19e complexes with intermediate indenyl-slipped rings such as [IndCpMo{P(OMe)$_3$}$_2$]$^{2+}$.[5] This shows that the indenyl slippage has a rather energetically shallow barrier and the slippage/bending of the ring is not limited to the discrete extreme forms of coordination η^5 or η^3. Rather, the redox-induced slippage responds in a subtle fashion to the need of accommodating the excess of electronic charge on the metal. Therefore, **1**$^-$ can be described as [IndMo^I(CO)$_2$(*p*-tolDAB$^\bullet$)]$^-$ with the extra charge partially localized on the DAB ligand and the other

(16) Bildstein, B.; Malaun, M.; Kopacka, H.; Fontani, M.; Zanello, P. *Inorg. Chim. Acta* **2000**, *300*, 16.
(17) Záliš, S.; Farrel, I. R.; Vlček, A., Jr. *J. Am. Chem. Soc.* **2003** *125*, 4580.
(18) Ackermann, M. N.; Kiihne, S. R.; Saunders, P. A.; Barnes, C. E.; Stallings, S. C.; Kim, H.; Woods, C.; Lagunoff, M. *Inorg. Chim. Acta* **2002**, *334*, 193.
(19) Tyler, D. R. *Acc. Chem. Res.* **1991**, *24*, 4, 325.
(20) Braden, D. A.; Tyler, D. R. *Organometallics* **2000**, *19*, 3762 and references therein.

Table 7. Comparison of Electrochemical Data, Relative to Reduction Processes, for a Mo(II) Complex and a Re(I) Compound with Biquinoline Bonded to the Metal

complex	$E_{1/2}$(1) (V)	E_c(2) (V)[a]	ref
[IndMo^{II}(CO)$_2$(Biq)]$^+$	−0.690 (rev)	−1.12 (irr)	this work
[Re^I(CO)$_3$(Biq)(pyz)]$^+$	−0.590 (rev)	−1.16 (qrev)	15
[Re^I(CO)$_3$(Biq)Br]	−0.940 (rev)	−1.29 (irr)	16

[a] E_c = cathodic potential.

part accommodated in the metal with concomitant partial indenyl slippage to a formal 4e donor.

Another interesting complex is [IndMo(CO)$_2$(biq)]$^+$ (**3**), which also shows a reversible reduction at a potential lower than that of **1** and a second irreversible reduction at −1.12 V. According to studies made for Re complexes, biquinoline is a ligand with a π-system sufficiently large to support two successive biq-centered 1e reductions.[21] The reduction potentials obtained in our study are quite similar to those observed for the Re(I) complexes [Re^I(CO)$_3$(Biq)(pyz)]$^+$ and [Re^I(CO)$_3$(Biq)Br] in Table 7.[21,22]

Although no DFT calculations were performed for complexes **2**−**5**, their reduction processes can tentatively be assigned to similar reduction processes to that of **1,** although with increasing irreversibility for the second reduction process.

Conclusion

Thirteen complexes of the type [IndMo(CO)$_2$(α-diimine)]$^+$ were prepared. In contrast to related species such as [IndMo(CO)$_2$(NCMe)$_2$]$^+$, none of them add NCMe in NCMe solution to produce detectable (^{1}H NMR) ring-slipped octahedral complexes [(η^3-Ind)Mo(CO)$_2$(α-diimine)(NCMe)]$^+$. The possibility of redox-induced indenyl slippage was tested by electrochemical reduction of the 13 [IndMo(CO)$_2$(α-diimine)]$^+$ complexes. The complex [IndMo(CO)$_2$(*p*-tolDAB)]$^+$ is unique in undergoing two successive, reversible 1e reductions. DFT calculations of the UV−vis spectrum of the three species of its model analogue [IndMo(CO)$_2$(phDAB)]$^{+/0/-}$ agree fairly well with the experimental UV−vis spectrum of the reduced [IndMo(CO)$_2$(*p*-tolDAB)]$^+$. These calculations show that the first reduction takes place at the DAB ligand without any hapticity change of the indenyl ring. Computation predicts that the second reduction generates a ring-slipped species, which is intermediate between η^5 and η^3 coordination. Such a species is, however, too unstable to isolate and decomposes with DAB ligand loss. The irreversibility of the reductive electrochemical processes observed in the majority of the other complexes studied prevents the straightforward extension of the conclusions drawn for complex **1** to the other [IndMo(CO)$_2$(α-diimine)]$^+$ compounds. Nevertheless, these results present an interesting case where the first reduction of an 18e η^5-indenyl cation leaves the metal unreduced with an unchanged η^5-indenyl. The more typical shallow profile of indenyl slippage, however, emerges upon the addition of a second electron.

Experimental Section

All experiments were carried out under an inert atmosphere of nitrogen using Schlenk techniques. Low-temperature reactions were performed using a 2-propanol/liquid nitrogen bath. Solvents were dried by standard procedures: diethyl ether, THF, hexane, and dimethoxyethane were dried over sodium wire and benzophenone ketyl under reflux and distilled, dichloromethane and acetonitrile were distilled under nitrogen over CaH_2 and kept respectively over 4 and 3 Å molecular sieves, and triethylamine was dried over CaH_2 and distilled. For all electrochemical studies only freshly distilled solvents were used. The compounds 2,2'-biquinoline, 5,6-ph$_2$-3-(2-py)-1,2,4-triazine, 4,4'-ph$_2$-2,2′-bpy, 1,10-phenanthroline, 4,7-ph$_2$-1,10-phenanthroline, 4,7-me$_2$-1,10-phenanthroline, 2-(2-pyridyl)-benzimidazole, and 1,2-Ph(NH$_2$)$_2$ were used as received from Aldrich. 1,4-*p*-tol-DAB, 1,4-cyclohexylDAB,[23] and benzimidazole[24] were synthesized according to the literature.

Synthesis of [η^5-IndMo(CO)$_2$(*p*-tol-DAB)]BF$_4$ (1). A solution of IndMo(η^3-C$_3$H$_5$)(CO)$_2$ (0.50 g, 1.6 mmol) in CH_2Cl_2 was treated with HBF$_4$·Et$_2$O (1 equiv). After 10 min, an excess of dme was added and the reaction mixture was left for 15 min. A 0.47 g portion (2 mmol) of *p*-tol-DBD was added, and the reaction mixture was left for 2 h at room temperature. After concentration to about 5 mL and addition of hexane, a dark purple complex precipitated. The mixture was filtered and the residue recrystallized from CH_2Cl_2/hexane.

Yield: 90%. Anal. Found: C, 54.21; N, 4.46; H, 3.71. Calcd: C, 54.94; N, 4.75; H, 3.91. IR (KBr, cm^{-1}): 2923 (w), 2019 (vs, C≡O), 1976 (vs, C≡O), 1513 (m), 1459 (m), 1445 (m), 1062 (vs B−F). ^{1}H NMR (CD_2Cl_2, 25 °C, δ in ppm): 7.94 (s, 2H, NCH), 7.38 (d, $^3J_{mo}$ = 8.1, 4H, H^{12}), 7.32 (m, $^3J_{H^7H^8}$ = 6.6, $^4J_{H^7H^5}$ = 3.0, 2H, H^{6,7}), 7.24 (d, $^3J_{om}$ = 8.1, 4H, H^{11}), 7.12 (m, $^3J_{H^8H^7}$ = 6.6, $^4J_{H^8H^6}$ = 3.0, 2H, H^{5,8}), 6.09 (d, $^3J_{H^3H^2}$ = 2.9, 2H, H^{1,3}), 5.28 (t, $^3J_{H^2H^3}$ = 2.9 Hz, 1H, H^2), 2.48 (s, 6H, CH$_3$). ^{13}C{^{1}H} NMR (CD_2Cl_2, 25 °C, δ in ppm): 236.2 (CO), 155.4 (NCH), 152.6 (*i*-C of *p*-tolyl), 141.0 (*p*-C of *p*-tolyl), 131.4 (C^{6,7}), 130.5 (*m*-C of *p*-tolyl), 125.8 (C^{5,8}), 122.7 (*o*-C of *p*-tolyl), 116.0 (C^{4,9}), 89.4 (C^2), 81.8 (C^{1,3}), 21.2 (CH$_3$). ^{19}F NMR (CD_2Cl_2, 25 °C, δ in ppm): −74.5, −74.4. ^{11}B NMR (CD_2Cl_2, 25 °C, δ in ppm): −1.3.

Synthesis of [η^5-IndMo(CO)$_2$(CyDAB)]BF$_4$ (2). A solution of IndMo(η^3-C$_3$H$_5$)(CO)$_2$ (0.50 g, 1.6 mmol) in CH_2Cl_2 was treated with HBF$_4$·Et$_2$O (1 equiv). After 10 min an excess of dme was added and the reaction was left for 15 min. A 0.47 g portion (2 mmol) of cyclohexylDAB was added, and the reaction mixture was left for 2 h at room temperature. After concentration to about 5 mL and addition of hexane, a dark purple complex precipitated. The mixture was filtered and the residue recrystallized from CH_2Cl_2/hexane.

Yield: 90%. IR (KBr, cm^{-1}): 2932 (w), 2856 (w), 1994 (vs, C≡O), 1928 (vs, C≡O), 1083 (vs, B−F). ^{1}H NMR (CD_2Cl_2, 25 °C, δ in ppm): 7.95 (s, 2H, H^{16}), 7.50−7.39 (c, 4H, H$^{5-8}$), 6.06 (d, $^3J_{H^3H^2}$ = 2.2, 2H, H^{1,3}), 5.52 (t, $^3J_{H^2H^3}$ = 2.2 Hz, 1H, H^2), 2.30−1.00 (c, 10H, H$^{11-15}$). ESI/MS (positive mode, *m*/*z*): 489.1 [(M$^{\bullet+}$, IndMo(CO)$_2$(CyDAB)$^{\bullet+}$], 461.1 (M$^{\bullet+}$ − 28, IndMo(CO)(CyDAB)$^{\bullet+}$]

Synthesis of [η^5-IndMo(CO)$_2$(2,2'-biq)]BF$_4$ (3). A solution of IndMo(η^3-C$_3$H$_5$)(CO)$_2$ (0.27 g, 0.87 mmol) in CH_2Cl_2 was treated with HBF$_4$·Et$_2$O (1 equiv). After 10 min an excess of dme was added and the reaction mixture was left for 15 min. A 0.33 g portion (0.84 mmol) of 2,2′-biquinoline was added, and the reaction mixture was left for 2 h at room temperature. After concentration to about 5 mL and addition of Et$_2$O, a deep blue complex precipitated. The mixture was filtered and the residue recrystallized from CH_2Cl_2/Et$_2$O.

Yield: 90%. Anal. Found: C, 57.23; N, 4.55; H, 3.15. Calcd: C, 57.08; N, 4.59; H, 3.14. IR (KBr, cm^{-1}): 1978 (vs, C≡O), 1958 (vs, C≡O), 1898 (vs, C≡O), 1879 (vs, C≡O), 1599 (s), 1510 (s), 1063 (vs, B−F). ^{1}H NMR (CD_2Cl_2, 25 °C, δ in ppm): 9.29 (d,

(21) Lin, R.; Fu, Y.; Brock, C. P.; Garr, T. F. *Inorg. Chem.* **1992**, *31*, 4346.

(22) Moya, S. A.; Guerrero, J.; Pastene, R.; Schmidt, R.; Sariego, R. *Inorg. Chem.* **1994**, *33*, 2341.

(23) (a) van Koten, G.; Vrieze, K. *Advances in Organometallic Chemistry*; Academic Press: New York, 1982; Vol. 21. (b) Colton, R.; Tomkins, I. B. *Aust. J. Chem.* **1965**, *18*, 447.

(24) Brady, J. E.; Fogarty, M. A. *J. Inorg. Nucl. Chem.* **1971**, *33*, 2706.

$^3J_{H^{11}H^{12}}$ = 5.9, 2H, H^{11}), 8.43 (d, $^3J_{H1^7H^{16}}$ = 1.9, 2H, H^{17}), 7.78, 7.52 (c, 8H, $H^{12-14,16}$), 6.99, 6.71 (m, $^3J_{H^8H^7}$ = 6.2, $^4J_{H^8H^6}$ = 2.9, 4H, H^{5-8}), 6.37 (d, $^3J_{H^3H^2}$ = 2.9, 2H, $H^{1,3}$), 5.34 (t, $^3J_{H^2H^3}$ = 2.9 Hz, 1H, H^2).

Synthesis of [η^5-IndMo(CO)$_2$(5,6-ph$_2$-3-(2-py)-1,2,4-triazine)]-BF$_4$ (4). A solution of IndMo(η^3-C_3H_5)(CO)$_2$ (0.50 g, 1.6 mmol) in CH_2Cl_2 was treated with HBF_4·Et_2O (1 equiv). After 10 min an excess of dme was added and the reaction mixture was left for 15 min. A 0.62 g portion (2 mmol) of 5,6-diphenyl-3-(2-pyridyl)-1,2,4-triazine was added, and the reaction mixture was left for 2 h at room temperature. After concentration to about 5 mL and addition of hexane, a purple complex precipitated. The mixture was filtered and the residue recrystallized from CH_2Cl_2/hexane.

Yield: 90%. Anal. Found: C, 55.77 N, 8.68; H, 3.22. Calcd: C, 56.05; N, 8.43; H, 3.19. IR (KBr, cm^{-1}): 1982 (vs, C≡O), 1899 (vs, C≡O), 1372 (m), 1057 (vs, B−F), 772 (w), 700 (w). ^{1}H NMR (CD_2Cl_2, 25 °C, δ in ppm): 9.45 (d, $^3J_{H^{29}H^{28}}$ = 5.9, 1H, H^{29}), 8.74 (d, $^3J_{H^{26}H^{27}}$ = 8.2, 1H, H^{26}), 8.16 (dd, $^3J_{H^{27}H^{26}}$ = 8.2, $^3J_{H^{27}H^{28}}$ = 7.8, 1H, H^{27}), 7.81 (dd, $^3J_{H^{28}H^{27}}$ = 7.8, 1H, H^{28}), 7.71−7.42 (c, 14H, $H^{10-15+19-23}$), 7.08 (d, $^3J_{H^5H^6}$ = 8.2, $^4J_{H^5H^7}$ = 1.5, 1H, H^5), 6.90 (d, $^3J_{H^8H^7}$ = 8.1, $^4J_{H^8H^6}$ = 1.6, 1H, H^8), 6.82 (c, 2H, $H^{6,7}$), 6.62 (m, 1H, H^3), 6.23 (m, 1H, H^1), 5.50 (dd, $^3J_{H^2H^1}$ = 3.0, $^3J_{H^2H^3}$ = 3.0 Hz, 1H, H^2). ^{13}C{^{1}H} NMR (CD_2Cl_2, 25 °C δ in ppm): 157.7 (C^{29}), 139.6 (C^{27}), 133.2, 131.8 ($C^{12,21}$), 130.6, 130.0, 129.6, 129.4 ($C^{10,11,13,14,19,20,22,23}$), 130.5, 129.2 ($C^{6,7}$), 128.1 ($C^{26}$), 127.9 ($C^{28}$), 126.7 ($C^5$), 125.7 ($C^8$), 91.1 ($C^2$), 80.5 ($C^3$), 80.3 ($C^1$).

Synthesis of [η^5-IndMo(CO)$_2$dppz]BF$_4$ (5). A solution of IndMo(η^3-C_3H_5)(CO)$_2$ (0.11 g, 0.35 mmol) in CH_2Cl_2 was treated with HBF_4·Et_2O (1 equiv). After 10 min an excess of dme was added and the reaction mixture was left for 15 min. A 0.09 g portion (0.31 mmol) of dppz was added, and the reaction mixture was left for 2 h at room temperature. After concentration to about 5 mL and addition of Et_2O, a ruby complex precipitated. The mixture was filtered and the residue recrystallized from CH_2Cl_2/Et_2O.

Yield: 75%. Anal. Found: C, 57.28; N, 3.62; H, 3.25. Calcd: ($^1/_2$ CH_2Cl_2): C, 57.09; N, 3.97; H, 3.43. Calcd: C, 54.75; N, 8.81; H, 2.69. IR (KBr, cm^{-1}): 1972 (vs, C≡O), 1899 (vs, C≡O), 1421 (w), 1384 (w), 1262 (w), 1083 (vs, B−F). ^{1}H NMR (CD_2Cl_2, 25 °C, δ in ppm): 9.79, 8.44, 8.10 (m, 10H, H^{10-17}), 7.00, 6.40 (m, 4H, H^{5-8}), 6.58 (d, 2H, $H^{1,3}$), 5.48 (t, 1H, H^2).

Synthesis of [η^5-IndMo(CO)$_2$ (4,4′-Ph$_2$-2,2′-bpy)]BF$_4$ (7). A solution of IndMo(η^3-C_3H_5)(CO)$_2$ (0.2, 0.65 mmol) in CH_2Cl_2 was treated with HBF_4·Et_2O (1 equiv). After 10 min an excess of dme was added and the reaction mixture was left for 15 min. A 0.25 g portion (0.8 mmol) of 4,4′-diphenyl-2,2′-bipy was added, and the reaction mixture was left for 2 h at room temperature. After concentration to about 5 mL and addition of Et_2O, a ruby complex precipitated. The mixture was filtered and the residue recrystallized from CH_2Cl_2/Et_2O.

Yield: 98%. Anal. Found: C, 59.86; N, 4.37; H, 3.40. Calcd: C, 59.85; N, 4.23; H, 3.50. IR (KBr, cm^{-1}): 1968 (vs, C≡O), 1886 (vs, C≡O), 1054 (B−F). ^{1}H NMR (CD_2Cl_2, 25 °C, δ in ppm): 9.35 (d, $^3J_{H^{10}H^{11}}$ = 6.2, 2H, H^{10}), 8.50 (c, 4H, $H^{11,13}$), 7.86 (c, 6H, H^{17-19}), 7.62 (d, $^3J_{H1^6H^{17}}$ = 5.1, 4H, $H^{16,20}$), 7.06, 6.80 (m, $^3J_{H^8H^7}$ = 6.6, $^4J_{H^8H^6}$ = 3.3, 4H, H^{5-8}), 6.43 (d, $^3J_{H^3H^2}$ = 2.2, 2H, $H^{1,3}$), 5.43 (t, $^3J_{H^2H^3}$ = 2.2 Hz, 1H, H^2).

Synthesis of [η^5-IndMo(CO)$_2$(1,10-phen)]BF$_4$ (8). A solution of IndMo(η^3-C_3H_5)(CO)$_2$ (0.20 g, 0.65 mmol) in CH_2Cl_2 was treated with HBF_4·Et_2O (1 equiv). After 10 min an excess of dme was added and the reaction mixture was left for 15 min. A 0.14 g portion (0.8 mmol) of 1,10-phenanthroline was added, and the reaction mixture was left for 2 h at room temperature. After concentration to about 5 mL and addition of Et_2O, a ruby complex precipitated. The mixture was filtered and the residue recrystallized from CH_2Cl_2/Et_2O.

Yield: 90%. Anal. Found: C, 48.44; N, 4.10; H, 2.91. Calcd: C, 51.72; N, 5.24; H, 2.83. Calcd ($^1/_2$ CH_2Cl_2): C, 48.61; N, 4.82; H, 3.47. IR (KBr, cm^{-1}): 1970 (vs, C≡O), 1875 (vs, C≡O), 1430 (m), 1382 (m), 1062 (vs, B−F), 844 (s), 770 (m), 718 (s). ^{1}H NMR (CD_2Cl_2, 25 °C, δ in ppm): 9.74 (d, $^3J_{H^{10}H^{11}}$ = 8.1, 2H, H^{10}), 8.58 (d, $^3J_{H^{12}H^{11}}$ = 8.1, 2H, H^{12}), 8.02 (s, 2H, H^{14}), 7.99 (dd, $^3J_{H^{11}H^{10}}$ = 8.1, $^3J_{H^{11}H^{12}}$ = 8.1, 2H, H^{11}), 6.88, 6.33 (m, $^3J_{H^8H^7}$ = 6.6, $^4J_{H^8H^6}$ = 3.3, 4H, H^{5-8}), 6.52 (d, $^3J_{H^3H^2}$ = 2.6, 2H, $H^{1,3}$), 5.44 (t, $^3J_{H^2H^3}$ = 2.6 Hz, 1H, H^2). ESI/MS (positive mode, *m*/*z*): 448.8 [($M^{\bullet+}$, IndMo(CO)$_2$(1,10-phen)$^{\bullet+}$].

Synthesis of [η^5-IndMo(CO)$_2$(4,7-ph$_2$-1,10-phe)]BF$_4$ (9). A solution of IndMo(η^3-C_3H_5)(CO)$_2$ (0.20 g, 0.65 mmol) in CH_2Cl_2 was treated with HBF_4·Et_2O (1 equiv). After 10 min an excess of dme was added and the reaction mixture was left for 15 min. A 0.27 g portion (0.8 mmol) of 4,7-diphenyl-1,10-phenanthroline was added, and the reaction mixture was left for 2 h at room temperature. After concentration to about 5 mL and addition of Et_2O, a ruby complex precipitated. The mixture was filtered and the residue recrystallized from CH_2Cl_2/Et_2O.

Yield: 90%. Anal. Found: C, 57.28; N, 3.62; H, 3.25. Calcd: ($^1/_2$ CH_2Cl_2): C, 57.09; N, 3.97; H, 3.43. IR (KBr, cm^{-1}): 3100 (w), 1970 (vs, C≡O), 1872 (vs, C≡O), 1426 (w), 1383 (w), 1230 (w), 1062 (vs, B−F), 763 (m), 703 (m). ^{1}H NMR (CD_2Cl_2, 25 °C, δ in ppm): 9.76 (d, $^3J_{H^{10}H^{11}}$ = 5.6, 2H, H^{10}), 8.02 (s, 2H, H^{20}), 7.92 (d, $^3J_{H^{11}H^{10}}$ = 5.6, 2H, H^{11}), 7.60 (c, 10H, H^{14-18}), 7.05, 6.47 (m, $^3J_{H^8H^7}$ = 6.7, $^4J_{H^8H^6}$ = 3.0, 4H, H^{5-8}), 6.60 (d, $^3J_{H^3H^2}$ = 3.0, 2H, $H^{1,3}$), 5.48 (t, $^3J_{H^3H^2}$ = 3.0 Hz, 1H, H^2). ESI/MS (positive mode, *m*/*z*): 600.98 [($M^{\bullet+}$, IndMo(CO)$_2$(4,7-ph$_2$-1,10-phen)$^{\bullet+}$], 572.8 [($M^{\bullet+}$ − 28, IndMo(CO)(4,7-ph$_2$-1,10-phen)$^{\bullet+}$], 544.9 [($M^{\bullet+}$ − 56, IndMo(4,7-ph$_2$-1,10-phen)$^{\bullet+}$].

Synthesis of [η^5-IndMo(CO)$_2$(4,7-Me$_2$-1,10-phen)]BF$_4$ (10). A solution of IndMo(η^3-C_3H_5)(CO)$_2$ (0.20 g, 0.65 mmol) in CH_2Cl_2 was treated with HBF_4·Et_2O (1 equiv). After 10 min an excess of dme was added and the reaction mixture was left for 15 min. A 0.17 g portion (0.8 mmol) of 4,7-dimethyl-1,10-phenanthroline was added, and the reaction mixture was left for 2 h at room temperature. After concentration to about 5 mL and addition of Et_2O, a red complex precipitated. The mixture was filtered and the residue recrystallized from CH_2Cl_2/Et_2O.

Yield: 90%. Anal. Found: C, 49.37; N, 4.74; H, 3.73. Calcd: C, 53.4; N, 5.0; H, 3.40. Calcd ($^1/_4$ CH_2Cl_2): C, 50.0 N, 4.80; H, 3.37. IR (KBr, cm^{-1}): 1970 (vs, C≡O), 1873 (vs, C≡O), 1423 (w), 1383 (w), 1058 (vs, B−F), 841 (w). ^{1}H NMR (CD_2Cl_2, 25 °C, δ in ppm): 9.44 (d, $^3J_{H^{10}H^{11}}$ = 5.5, 2H, H^{10}), 8.06 (s, 2H, H^{14}), 7.70 (d, $^3J_{H^{11}H^{10}}$ = 5.5, 2H, H^{11}), 6.81, 6.28 (m, $^3J_{H^8H^7}$ = 6.6, $^4J_{H^8H^6}$ = 3.3, 4H, H^{5-8}), 6.39 (d, $^3J_{H^3H^2}$ = 2.6, 2H, $H^{1,3}$), 5.36 (t, $^3J_{H^3H^2}$ = 2.6 Hz, 1H, H^2), 2.86 (s, 6H, CH_3).

Synthesis of [η^5-IndMo(CO)$_2$(2-(2-pyridyl)benzimidazole)]BF$_4$ (11). A solution of IndMo(η^3-C_3H_5)(CO)$_2$ (0.20 g, 0.65 mmol) in CH_2Cl_2 was treated with HBF_4·Et_2O (1 equiv). After 10 min an excess of dme was added and the reaction mixture was left for 15 min. A 0.16 g portion (0.8 mmol) of 2-(2-pyridyl)benzimidazole was added, and the reaction mixture was left for 2 h at room temperature. After concentration to about 5 mL and addition of Et_2O, a red complex precipitated. The mixture was filtered and the residue recrystallized from CH_2Cl_2/Et_2O.

Yield: 90%. Anal. Calcd: C, 50.30; N, 7.65; H, 2.94. IR (KBr, cm^{-1}): 1968 (vs, C≡O), 1887 (vs, C≡O), 1453 (vs), 1083 (vs, B−F). ^{1}H NMR (CD_2Cl_2, 25 °C, δ in ppm): 11.10 (br, 1H, NH), 9.18, 8.97, 7.91, 6.72, 6.61 (m, 8H, $H^{10-13+17-20}$), 8.31, 7.72 (d, 2H, H^{5+8}), 7.41, 7.33 (dd, 2H, H^{6+7}), 6.46, 6.33, 6.23 (m, 3H, H^{1-3}). ESI/MS (positive mode, *m*/*z*): 464.0 [($M^{\bullet+}$, IndMo(CO)$_2${2-(2-py)-benz}$^{\bullet+}$].

Synthesis of [η^5-IndMo(CO)$_2$(2,2′-biimidazole)]BF$_4$ (12). A solution of IndMo(η^3-C_3H_5)(CO)$_2$ (0.25 g, 0.81 mmol) in CH_2Cl_2 was treated with HBF_4·Et_2O (1 equiv). After 10 min an excess of dme was added and the reaction mixture was left for 15 min. A 0.13 g (1 mmol) portion of 2,2′-biimidazole was added, and the reaction mixture was left for 2 h at room temperature. After

concentration to about 5 mL and addition of Et_2O, an orange complex precipitated. The mixture was filtered and the residue recrystallized from CH_2Cl_2/Et_2O.

Yield: 90%. Anal. Found: C, 34.43; N, 11.4; H, 2.60. Calcd: C, 41.84; N, 11.48; H, 2.68. Calcd (2 CH_2Cl_2): C, 34.67; N, 8.51; H, 1.97. IR (KBr, cm^{-1}): 3130 (w), 1963 (vs, C≡O), 1880 (vs, C≡O), 1322 (w), 1084 (vs, B−F), 781 (m). ^{1}H NMR (CD_2Cl_2, 25 °C, δ in ppm): 11.6 (br, 2H, NH), 7.52, 7.22 (d, 4H, H^{10,11}), 6.94, 6.85 (m, $^3J_{H^8H^7}$ = 6.6, $^4J_{H^8H^6}$ = 3.3, 4H, H$^{5-8}$), 6.22 (d, $^3J_{H^3H^2}$ = 2.6, 2H, H^{1,3}), 5.23 (t, $^3J_{H^2H^3}$ = 2.6 Hz, 1H, H^2). ESI/MS (positive mode, *m*/*z*): 349.0 [(M$^{\bullet+}$, IndMo(CO)$_2$(2,2'-H$_2$BiimH)$^{\bullet+}$].

Synthesis of {η^5-IndMo(CO)$_2$[1,2-Ph(NH$_2$)$_2$]}BF$_4$ (13). A solution of IndMo(η^3-C$_3$H$_5$)(CO)$_2$ (0.23 g, 0.74 mmol) in CH_2Cl_2 was treated with HBF_4·Et_2O (1 equiv). After 10 min an excess of dme was added and the reaction mixture was left for 15 min. A 0.92 g portion (0.85 mmol) of 1,2-phenylenediamine was added, and the reaction mixture was left for 2 h at room temperature. A partially insoluble orange solid precipitated. and full precipitation of complex was obtained after addition of Et_2O.

Yield: 90%. Anal. Calcd: C, 44.2; N, 6.0; H, 3.2. IR (KBr, cm^{-1}): 1981 (vs, C≡O), 1965 (vs, C≡O), 1083 (vs, B−F). ^{1}H NMR (CD_2Cl_2, room temperature, δ in ppm): 7.59, 6.81 (m, $^3J_{H^8H^7}$ = 6.0, $^4J_{H^8H^6}$ = 3.0, 4H, H$^{5-8}$), 7.11, 7.02 (d, $^3J_{H^{12}H^{13}}$ = 1.9, 4H, H^{12,13}), 6.28 (d, $^3J_{H^3H^2}$ = 2.2, 2H, H^{1,3}), 5.73 (br, 4H, NH$_2$), 5.19 (t, $^3J_{H^2H^3}$ = 2.2 Hz, 1H, H$_2$). ESI/MS (positive mode, *m*/*z*): 375.0 [(M$^{\bullet+}$, IndMo(CO)$_2$(1,2-Ph(NH$_2$)$_2$)$^{\bullet+}$].

Electrochemical Measurements and UV−Vis Electronic Spectra. All solutions were prepared using freshly distilled dichloromethane (**1**−**12**) or dimethoxyethane (**13**); tetrabutylammonium tetrafluoroborate ($TBABF_4$) was used as the supporting electrolyte. Cyclic voltammetry was performed with a BAS CV/50 potentiostat/galvanostat, in a closed standard three-electrode electrochemical cell that kept the solution protected from air, in CH_2Cl_2/0.1 M $TBABF_4$ at a scan rate of 0.25 V. A BAS MF-2012 glassy-carbon electrode was used as the working electrode and a BAS MW-4130 electrode as the counter electrode. The measured potentials were not corrected for liquid junction potentials and are reported relative to that of the SCE reference electrode and to the $E_{1/2}$ value of the ferrocenium/ferrocene couple. Typically the complex solution was first cycled at the scan rate used until repetitive voltammograms were observed; this usually occurred after approximately five potential cycles for all the complexes, as exemplified for complex **1** in Figure 2.

Controlled-potential electrolysis of the complexes was performed with an Autolab PGSTAT 20 potentiostat/galvanostat. under an Ar atmosphere. The electrochemical cell has two compartments: one for the platinum-gauze working electrode and the other for the platinum-gauze counter electrode, which are separated by a silica frit. An Ag/AgCl (1 mol dm^{-3} NaCl) reference electrode was used. For compounds **2**−**4** electrolyses were performed at −1.25 V for 30 min, whereas for complex **1** (a 1 mM solution was used) the reduction was carried out in two stages: 10 min at −0.75 V and 20 min at a potential of −1.5 V. After reduction the electrolyzed solutions were transferred with a flux of Ar to an UV−vis cell to be used under an inert atmosphere and the UV−vis spectra were recorded on an Agilent 8453 diode array spectrophotometer; in the case of complex **1**, UV−vis spectra were also recorded after the first potential reduction. The electrolysis of the complexes and their UV spectra were performed in NCMe/0.1 M $TBABF_4$. The use of a solvent different from that for CV was dictated by the highly volatile nature of CH_2Cl_2, which prevented the easy transfer of the electrolyzed solutions under the high flux of Ar needed to avoid the oxidation of the highly unstable reduced species.

The electronic spectra of the complexes and free ligands were obtained in a 0.1 M $TBABF_4$ acetonitrile solution; the spectra of the latter compounds were recorded on a Varian Cary 3E spectrophotometer.

Single-Crystal X-ray Structure Determination of Compound 4. Crystal data: $C_{31}H_{21}BF_4MoN_4O_2$, M_r = 664.27, purple fragment (0.10 × 0.25 × 0.25 mm^3), monoclinic, $P2_1$ (No. 4), a = 8.6558(1) Å, b = 16.4150(3) Å, c = 10.0677(2) Å, β = 97.3783(6)°, V = 1418.62(4) Å^3, Z = 2, d_{calcd} = 1.555 g cm^{-3}, F_{000} = 668, μ = 0.525 mm^{-1}. Preliminary examination and data collection were carried out on a κ-CCD device (Nonius MACH3) with an Oxford Cryosystems cooling system at the window of a rotating anode (Nonius FR591) with graphite-monochromated Mo Kα radiation (λ = 0.710 73 Å). Data collection was performed at 123 K within the θ range of 2.37° < θ < 25.40°. A total of 24 425 reflections were integrated. Raw data were corrected for Lorentz and polarization and, arising from the scaling procedure, for latent decay and absorption effects. After merging (R_{int} = 0.043), 5188 (5010 with $I_o > 2\sigma(I_o)$) independent reflections remained, and all were used to refine 472 parameters. The structure was solved by a combination of direct methods and difference Fourier syntheses. All non-hydrogen atoms were refined with anisotropic displacement parameters. All hydrogen atoms were found and refined with individual isotropic displacement parameters. Full-matrix least-squares refinements were carried out by minimizing $\sum w(F_o^2 - F_c^2)^2$ and converged with R1 = 0.0233 ($I_o > 2\sigma(I_o)$), wR2 = 0.0465 (all data), GOF = 1.075, and a shift/error of <0.001. The final difference Fourier map showed no striking features ($\Delta e_{min/max}$ = +0.32/−0.27 e Å^{-3}). The correct enantiomer was proved by the Flack parameter ϵ = −0.02(2). All calculations were performed on an Intel Pentium II PC, with the STRUX-V system, including the programs PLATON, SIR92, and SHELXL-97.[25] Crystallographic data (excluding structure factors) for the structure reported in this paper have been deposited with the Cambridge Crystallographic Data Centre as Supplementary Publication no. CCDC-XXXXXX (**4**). Copies of the data can be obtained free of charge on application to the CCDC, 12 Union Road, Cambridge CB2 1EZ, U.K. (fax, (+44)1223-336-033; e-mail, deposit@ccdc.cam.ac.uk).

DFT Calculations. Density functional theory calculations[26] were performed using the Amsterdam Density Functional program package (ADF2002).[27] The local spin density (LSD) exchange correlation potential was used with the local density approximation of the correlation energy (Vosko−Wilk−Nusair).[28] Full geometry optimizations, without any symmetry constraints, were performed using the generalized gradient approximation[29] (Becke's exchange[30]

(25) (a) Data Collection Software for NONIUS κ-CCD Devices; Nonius, Delft, The Netherlands, 1997. (b) Otwinowski, Z.; Minor, W. *Methods Enzymol.* **1997,** *276*, 307ff. (c) Hahn, T., Wilson, A. J. C., Eds. *International Tables for Crystallography*, 3rd ed.; Kluwer Academic: Dordrecht, Boston, London, 1992; Vol. C. (d) Artus, G.; Scherer, W.; Priermeier, T.; Herdtweck, E. STRUX-V: A Program System to Handle X-ray Data; TU München, Garching, Germany, 1997. (e) Spek, A. L. PLATON: A Multipurpose Crystallographic Tool; Utrecht University, Utrecht, The Netherlands, 2001. (f) Altomare, A.; Cascarano, G.; Giacovazzo, C.; Guagliardi, A.; Burla, M. C.; Polidori, G.; Camalli, M. SIR92. *J. Appl. Crystallogr.* **1994**, *27*, 435−436. (g) Sheldrick, G. M. SHELXL-97; University of Göttingen, Göttingen, Germany, 1998.

(26) Parr, R. G.; Yang, W. *Density Functional Theory of Atoms and Molecules*; Oxford University Press: New York, 1989.

(27) (a) Baerends, E. J.; Bérces, A.; Bo, C.; Boerrigter, P. M.; Cavallo, L.; Deng, L.; Dickson, R. M.; Ellis, D. E.; Fan, L.; Fischer, T. H.; Fonseca Guerra, C.; van Gisbergen, S. J. A.; Groeneveld, J. A.; Gritsenko, O. V.; Harris, F. E.; van den Hoek, P.; Jacobsen, H.; van Kessel, G.; Kootstra, F.; van Lenthe, E.; Osinga, V. P.; Philipsen, P. H. T.; Post, D.; Pye, C. C.; Ravenek, W.; Ros, P.; Schipper, P. R. T.; Schreckenbach, G.; Snijders, J. G.; Sola, M.; Swerhone, D.; te Velde, G.; Vernooijs, P.; Versluis, L.; Visser, O.; van Wezenbeek, E.; Wiesenekker, G.; Wolff, S. K.; Woo, T. K.; Ziegler, T. ADF-2002; SCM: Amsterdam, 2002. (b) Baerends, E. J.; Ellis, D.; Ros, P. *Chem. Phys.* **1973**, *2*, 41. (c) Baerends, E. J.; Ros, P. *Int. J. Quantum Chem.* **1978**, *S12*, 169. (d) Boerrigter, P. M.; te Velde, G.; Baerends, E. J. *Int. J. Quantum Chem.* **1988**, *33*, 87. (e) te Velde, G.; Baerends, E. J. *J. Comput. Phys.* **1992**, *99*, 84.

(28) Vosko, S. H.; Wilk, L.; Nusair, M. *Can. J. Phys.* **1980**, *58*, 1200.

(29) (a) Versluis, L.; Ziegler, T. *J. Chem. Phys.* **1988**, *88*, 322. (b) Fan, L.; Ziegler, T. *J. Chem. Phys.* **1991**, *95*, 7401.

(30) Becke, A. D. *Phys. Rev. A* **1988**, *38*, 3098.

and Perdew's[31] correlation functionals). Relativistic effects were treated with the ZORA approximation.[32] Spin-unrestricted calculations were performed for the paramagnetic species.

The core orbitals were frozen for Mo ([1−4]s, [2−3]p, 3d), C, N, and O (1s). Triple-ζ Slater-type orbitals (STO) were used to describe the valence shells C, O, N (2s and 2p) and Mo (4d, 5s). One polarization function was added to C, O, N (single-ζ, 3d) and Mo (single-ζ, 5p).

TD-DFT calculations (ADF)[33] were performed for the diamagnetic model complexes $\mathbf{1m}^+$ and $\mathbf{1m}^-$**.** TD-DFT[15] calculations were also performed using the Gaussian98 package[34] on the ADF optimized geometries for the three models. Since the results from both programs were qualitatively the same, only the Gaussian results are discussed in the text. The hybrid B3LYP[35] functional was adopted for all TD-DFT calculations. The standard LANL2DZ[36] basis set along with the associated ECP was used for Mo, while a standard 6-31G(d) basis set[37] was used for C, O and N, and the 3-21G basis set was taken for H.[38] Spin-unrestricted calculations were performed for the paramagnetic species.

Graphical representations of molecular orbitals were drawn with MOLEKEL.[39]

Acknowledgment. This work was financed by the FCT through Project POCTI /QUI/36127/2000. C.C.L.P. and P.J.C. thank the FCT for grants. We thank E. Melo for the use of his spectrophotometric facilities.

Supporting Information Available: Tables of atomic coordinates, atomic displacement parameters, and bond distances and angles for complex **4**; a CIF file also gives the crystal data. This material is available free of charge via the Internet at http://pubs.acs.org.

OM050986R

(31) Perdew, J. P. *Phys. Rev. B* **1986**, *33*(12), 8822.

(32) van Lenthe, E.; Ehlers, A.; Baerends, E. J. *J. Chem. Phys*. **1999**, 110, 8943.

(33) (a) van Gisbergen, S. J. A.; Groeneveld, J. A.; Rosa, A.; Snijders, J. G.; Baerends, E. J. *J. Phys. Chem.* **1999**, *103A*, 6835. (b) Rosa, A.; Baerends, E. J.; van Gisbergen, S. J. A.; van Lenthe, E.; Groeneveld, J. A.; Snijders, J. G. *J. Am. Chem. Soc*. **1999**, *121*, 10356. (c) van Gisbergen, S. J. A.; Rosa, A.; Ricciardi, G.; Baerends, E. J. *J. Chem. Phys.* **1999**, *111*, 2499.

(34) Frisch, M. J.; Trucks, G. W.; Schlegel, H. B.; Scuseria, G. E.; Robb, M. A.; Cheeseman, J. R.; Zakrzewski, V. G.; Montgomery, Jr., J. A.; Stratmann, R. E.; Burant, J. C.; Dapprich, S.; Millam, J. M.; Daniels, A. D.; Kudin, K. N.; Strain, M. C.; Farkas, O.; Tomasi, J.; Barone, V.; Cossi, M.; Cammi, R.; Mennucci, B.; Pomelli, C.; Adamo, C.; Clifford, S.; Ochterski, J.; Petersson, G. A.; Ayala, P. Y.; Cui, Q.; Morokuma, K.; Rega, N.; Salvador, P.; Dannenberg, J. J.; Malick, D. K.; Rabuck, A. D.; Raghavachari, K.; Foresman, J. B.; Cioslowski, J.; Ortiz, J. V.; Baboul, A. G.; Stefanov, B. B.; Liu, G.; Liashenko, A.; Piskorz, P.; Komaromi, I.; Gomperts, R.; Martin, R. L.; Fox, D. J.; Keith, T.; Al-Laham, M. A.; Peng, C. Y.; Nanayakkara, A.; Challacombe, M.; Gill, P. M. W.; Johnson, B.; Chen, W.; Wong, M. W.; Andres, J. L.; Gonzalez, C.; Head-Gordon, M.; Replogle, E. S.; Pople, J. A. *Gaussian 98*, Revision A.11.3; Gaussian, Inc., Pittsburgh, PA, 2002.

(35) (a) Lee, C.; Yang, W.; Parr, R. G. *Phys. Rev. B* **1988**, *37*, 785. (b) Becke, A. D. *J. Chem. Phys.* **1993**, *98*, 5648.

(36) (a) Dunning, T. H., Jr.; Hay, P. J. In *Modern Theoretical Chemistry*; Shaefer, H. F., III, Ed.; Plenum Press: New York, 1977; Vol. 3, pp 1−27. (b) Hay, P. J.; Wadt, W. R. *J. Chem. Phys.* **1985**, *82*, 270. (c) Hay, P. J.; Wadt, W. R. *J. Chem. Phys.* **1985**, *82*, 299.

(37) (a) Ditchfield, R.; Hehre, W. J.; Pople, J. A. *J. Chem. Phys.* **1971**, *54*, 724. (b) Hehre, W. J.; Ditchfield, J. A.; Pople, J. A. *J. Chem. Phys.* **1972**, *56*, 2257. (c) Hariharan, P. C.; Pople, J. A. *Theor. Chim. Acta* **1973**, *28*, 213. (d) Hariharan, P. C.; Pople, J. A. *Mol. Phys.* **1974**, *27*, 209. (e) Gordon, M. S. *Chem. Phys. Lett.* **1980**, *76*, 163.

(38) Binkley, J. S.; Pople, J. A.; Hehre, W. J. *J. Am. Chem. Soc.* **1980**, *102*, 939.

(39) Portmann, S.; Lüthi, H. P. *Chimia* **2000**, *54*, 766.